




Experimental investigation of the period-adding bifurcation route to chaos in plasmaZijia Chu ¹, Jingfeng Yao ^{1,2,3,*}, Hailu Wang,⁴ Chengxun Yuan ^{1,2,3,†}, Zhongxiang Zhou,^{1,2,3}
Anatoly Kudryavtsev,^{1,2,3} Ying Wang,^{1,2,3} and Xiaou Wang^{1,2,3}¹*School of Physics, Harbin Institute of Technology, Harbin 150001, People's Republic of China*²*Heilongjiang Provincial Key Laboratory of Plasma Physics and Application Technology, Harbin 150001, China*³*Heilongjiang Provincial Innovation Research Center for Plasma Physics and Application Technology, Harbin 150001, People's Republic of China*⁴*Institute of Defense Engineering, AMS, PLA, Luoyang 471023, China*

(Received 31 May 2023; accepted 7 November 2023; published 27 November 2023)

Since the characteristic timescales of the various transport processes inside the discharge plasma span several orders of magnitude, it can be regarded as a typical fast-slow system. Interestingly, in this work, a special kind of complex oscillatory dynamics composed of a series of large-amplitude relaxation oscillations and small-amplitude near-harmonic oscillations, namely, mixed-mode oscillations (MMOs), was observed. By using the ballast resistance as the control parameter, a period-adding bifurcation sequence of the MMOs, i.e., from L^s to L^{s+1} , was obtained in a low-pressure DC glow discharge system. Meanwhile, a series of intermittently chaotic regions caused by inverse saddle-node bifurcation was embedded between the two adjacent periodic windows. The formation mechanism of MMOs was analyzed, and the results indicated that the competition between electron production and electron loss plays an important role. Meanwhile, the nonlinear time series analysis technique was used to study the dynamic behavior quantitatively. The attractor in the reconstructed phase space indicated the existence of the homoclinic orbits of type Γ^- . In addition, by calculating the largest Lyapunov exponent (LLE), the chaotic nature of these states was confirmed and quantitatively characterized. With the decrease in the ballast resistance, the return map of the chaotic state gradually changed from the nearly one-dimensional single-peak structure to the multibranch structure, which indicates that the dissipation of the system decreased. By further calculating the correlation dimension, it was shown that the complexity of the strange attractors increased for higher-order chaotic states.

DOI: [10.1103/PhysRevE.108.055210](https://doi.org/10.1103/PhysRevE.108.055210)**I. INTRODUCTION**

It is widely believed that a nonlinear physical system far from the thermodynamic equilibrium state can exhibit complex dynamic behavior with regular or irregular structures in the time and/or space domains. The existence of deterministic chaos in laboratory plasmas has been extensively demonstrated both experimentally and numerically over the last decades [1–6]. Due to the existence of the negative differential conductivity (NDC), the discharge plasmas working in the subnormal glow discharge regime can yield the development of self-sustained oscillations regardless of the presence of the external driving forces, which can be observed by recording the macroscopic electrical signals [7–9]. The charge-breakdown-discharge process is repeated within the system during the manifestation of self-sustained oscillation. Meanwhile, it has been also suggested that a variety of complex bifurcations can be observed as the discharge parameter changes. Several transition routes to chaos have been reported, such as the period-doubling bifurcation sequence [10–13], the

quasiperiodicity route [4,14–16], and the intermittent chaos route [17–19].

In recent years, the research on nonlinear science has mainly focused on the complex oscillatory dynamics in more complex and realistic physical systems with multiple timescales [20–23]. Since different mechanisms are active during different phases of the system evolution, the system will alternately undergo slow and fast motion, which will cause a special periodic oscillatory state, namely, mixed-mode oscillations (MMOs). The typical characteristic of MMOs is that an oscillation period contains L large-amplitude oscillations (LAOs) followed by s small-amplitude oscillations (SAOs). The corresponding oscillatory state is denoted by L^s . The difference in the amplitude between LAOs and SAOs is typically more than an order of magnitude. Since the first discovery of MMOs in the Belousov-Zhabotinsky reaction, it has been widely observed in electrochemical systems [24–26], electric circuits [27–29], biological systems [30,31], laser dynamics [32–34], and many other physical systems [35,36].

During the alternating periodic-chaotic (APC) sequence, as the name implies, the system will alternately exhibit both periodic and chaotic oscillations with the change in the control parameters. This process can be considered as a typical route to chaos of mixed-mode oscillations. As a typical dynamical system with multiple timescales for the participating

*yaojf@hit.edu.cn

†yuancx@hit.edu.cn

modes, however, there are only a few reports in the literature on the APC in the discharge plasmas. The first experimental observation of APC in discharge plasmas was reported by Braun *et al.* [37,38]. By changing the control parameter (which was the applied voltage in their work), an APC sequence due to the Shilnikov homoclinic orbit losing its stability was obtained. The numerical simulation of the MMOs and the transition from periodic to chaotic oscillations was carried out by Hayashi by using a one-dimensional simple fluid model and coupling the external circuit as the boundary conditions [39]. In addition, the previously reported works focused on only reporting experimental phenomena and there is a lack of quantitative analysis of the oscillatory dynamics of the system. Therefore, a deep understanding of the dynamic characteristics of MMOs in discharge plasma systems is undoubtedly required. With the development of discrete time series analysis techniques, it is possible to quantitatively characterize complex oscillatory dynamics. Along these lines, the goal of this work is to provide qualitative knowledge of the characteristics of the MMOs in the discharge plasma system. A new APC bifurcation sequence of the MMOs was obtained in a low-pressure DC glow discharge system by varying the ballast resistance, while the other discharge parameters were fixed. The periodic windows caused by saddle-node bifurcation were ordered in an arithmetic series, i.e., from L^s to L^{s+1} , which is also known as the period-adding bifurcation. The appearance of the MMOs and the APC sequence was explained as a result of the competition between the electron production due to the inelastic collision ionization processes and the electron loss due to the directional movement process towards the anode. The time-series analysis tools, such as return maps, phase space reconstruction, correlation dimensions, and largest Lyapunov exponent were used to quantitatively analyze the chaotic dynamic characteristics of the strange attractor of the system.

This article is organized as follows: In Sec. II, a brief description of the experimental apparatus is presented. In Sec. III A, the mode transition processes of the dynamic behavior were thoroughly analyzed. By adjusting the ballast resistance, the period-adding bifurcation sequence with the alternating periodic-chaotic phenomenon is observed. In Sec. III B, the time-series analysis techniques are introduced to quantitatively analyze the oscillatory dynamics of the chaotic region. Finally, the conclusions are summarized in Sec. IV.

II. EXPERIMENTAL APPARATUS

In this work, the glow discharge was ignited between two cylindrical hollow molybdenum electrodes in a glass tube. The schematic diagram of the experimental setup with the geometry size marked is presented in Fig. 1. The experiments were performed with air as the background gas and the working pressure was pumped to $p = 15$ Pa. The cathode was grounded and the total voltage provided by a DC power supply was fixed at 2100 V. In some previously reported works in the literature, it has been demonstrated that when the control parameters such as the ballast resistance or applied voltage, are gradually changed, the dynamic behavior of the system will exhibit a simple—complex—simple transition during the

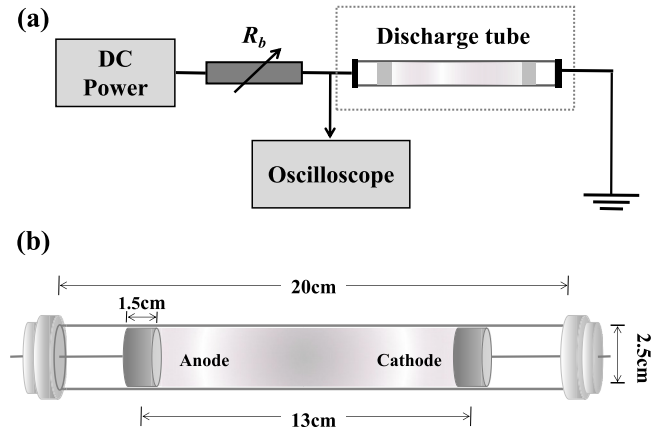


FIG. 1. (a) Schematic illustration of the experimental setup. (b) The geometry size of the discharge tube.

transition from the Townsend discharge to the glow discharge [12,40]. In our current experiment, a variable resistor (adjustable from 0.1 to 1000 M Ω) R_b was connected in series as a control parameter. The transition of the discharge from the Townsend discharge to the glow discharge regime can be achieved by adjusting the value of the ballast resistor. The time series of the discharge voltage was recorded by a digital oscilloscope (Keysight InfiniiVision 3034G) to characterize the dynamic behavior of the system.

III. RESULTS AND DISCUSSION

A. Observation of period-adding bifurcation to chaos

In this section, the variation of the dynamic behavior of the discharge system with the change in the control parameter was provided. The experiment was started at a fairly high ballast resistance (about several hundred M Ω). The system was therefore in a stationary Townsend discharge regime with a very low current. Figure 2 presents the time evolution of the discharge voltage at different ballast resistances. The period-adding bifurcation sequence of the system with the change in the control parameter, i.e., R_b , is described as follows: With the ballast resistance R_b decreased to about 100 M Ω , the stationary discharge state lost its stability through a Hopf bifurcation and the large amplitude relaxation oscillations appear, as shown in Fig. 2(a). This oscillatory state is named as 1^0 , where L^s indicates one oscillation period containing L LAOs and s SAOs as was mentioned above. The LAOs correspond to the repetitive charging, breakdown, discharging processes, which are microscopically manifested in the periodic formation and dissipation of the cathode sheath due to the existence of the negative differential conductivity [41–43]. With the gradual decrease in R_b , the frequency of the LAOs will be gradually increased due to the decrease in the characteristic time of the charging phase, which can be clearly identified in Fig. 2(b).

In addition, by comparing Fig. 2(a) with Fig. 2(b) and the insets, it can also be observed that there are significant differences in the shape of the single pulse, which could be explained as follows: The loss of electrons is mainly due to the electron flux towards the anode determined by the electric

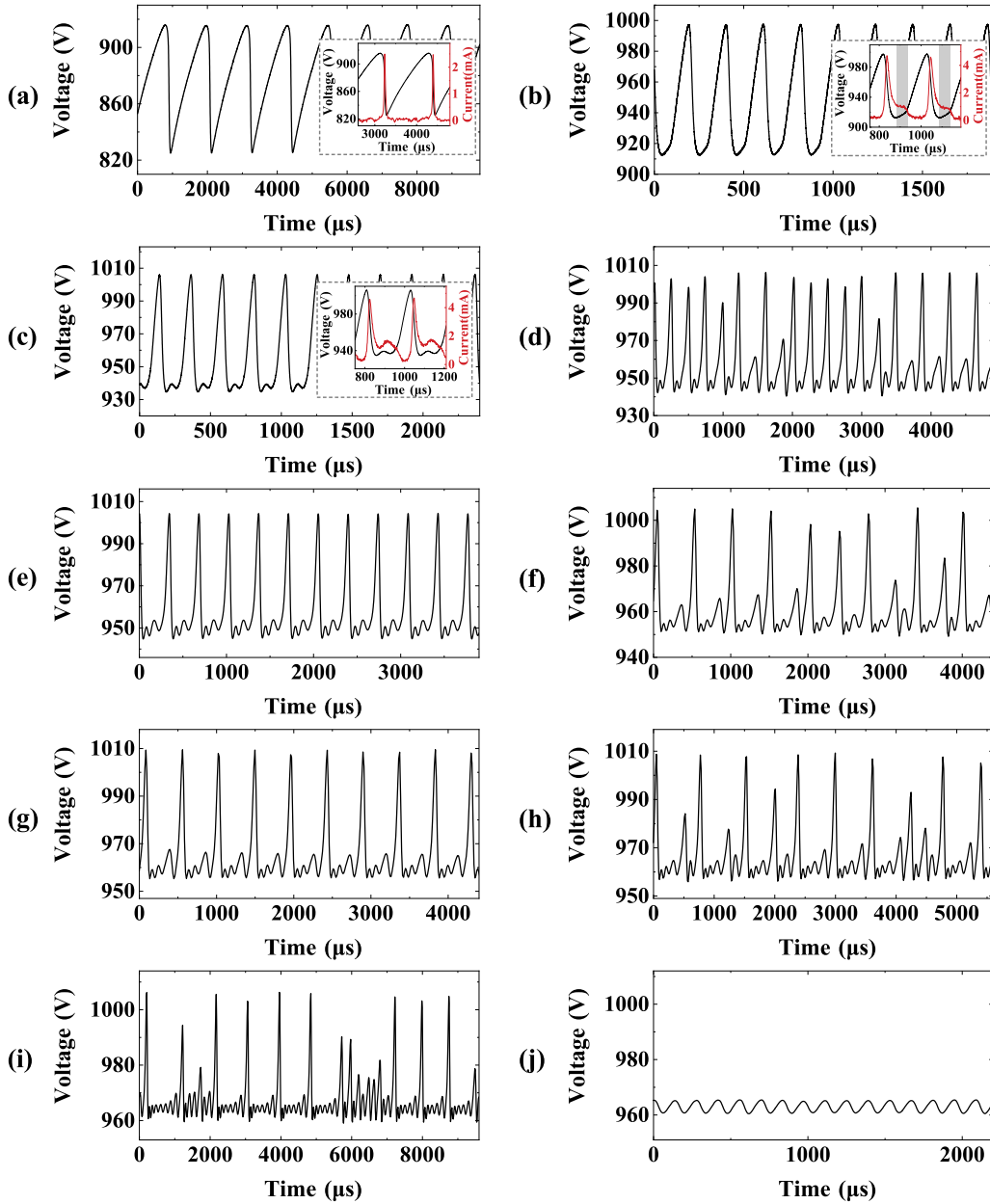


FIG. 2. The evolution of the discharge voltage at applied voltage $U_0 = 2100$ V and pressure $p = 15$ Pa for the different U_0 values of the ballast resistance (a) 1^0 : $R_b = 100$ MΩ, (b) 1^0 : $R_b = 25$ MΩ, (c) 1^1 : $R_b = 18.6$ MΩ, (d) $C^{(1,2)}$: $R_b = 16.8$ MΩ, (e) 1^2 : $R_b = 16.4$ MΩ, (f) $C^{(2,3)}$: $R_b = 15.9$ MΩ, (g) 1^3 : $R_b = 15.7$ MΩ, (h) $C^{(3,4)}$: $R_b = 15.5$ MΩ, (i) $C^{(n,n+1)}$: $R_b = 15.2$ MΩ, (j) 0^1 : $R_b = 15.1$ MΩ. The insets in panels (a)–(c) show the details of the voltage and current pulses in one period.

field and the density gradient while the production of electrons is mainly due to the inelastic collisional ionization processes, which corresponds to two characteristic timescales, namely the characteristic time of electron loss t_l and the characteristic time of electron production t_p , respectively. In the case of higher R_b , the lower input power results in a relatively lower electron density and inelastic collisional ionization frequency during the discharge phase. Therefore, t_p will be much higher than t_l and the electron production process could be negligible as a slow process during the current pulse phase. As shown in Fig. 2(a) and its inset, when the electrodes were charged to the peak voltage, the gas gap was broken and the voltage dropped rapidly by about 100 V. During this process, the electron

density first increased rapidly due to the electron avalanche and the cathode sheath structure was formed, and then decreased rapidly due to the end of the current pulse until the cathode sheath could no longer sustain and dissipate. Then the system was charged like a capacitor until the breakdown voltage was reached again and the above process was repeated.

On the other hand, the electron avalanche effect will be more significant in the discharge phase at lower R_b , leading to a higher electron density. Therefore, t_p is not much larger than t_l , and the inelastic collisional ionization process could not be considered as a slow process and ignored, which would weaken the electron loss. Therefore, the end of the falling edge in each period of the waveform is more gentler. Meanwhile, it

is worth noting that a relatively smooth rising edge appeared at the beginning of the charging phase compared with the case of high resistance [as shown in the gray area in the illustration of Fig. 2(b)]. During the smoother rising edge, the decrease in current density allowed the charging process to begin and the voltage to rise. However, there were still a relatively large number of electrons between the electrodes, sufficient to distort the electric field and inhibit the dissipation of the cathode sheath, which in turn hindered the voltage from rising.

The 1^0 state will be maintained until $R_b = 20.2 \text{ M}\Omega$. As R_b continues to decrease, there will be a critical value such that, before the end of the discharge phase (corresponding to the vicinity of the voltage nadir), t_p will gradually approach and finally become lower than t_l , where an 1^1 periodic state arises, as shown in Fig. 2(c) and the inset. In this case, although the current pulse is terminated and the voltage begins to rise gradually, the residual electron density remains high enough for further avalanche ionization, causing the electron density to rise again. When the electron density increases to a point where the electron-loss process dominates, the discharge process occurs again accompanied by a renewed drop in voltage. Note that the peak value of this pulse will be lower than the previous one due to the effect of the residual charge. Thus, we can observe the appearance of a SAO following the LAO. Subsequently, the residual charge particles are fully released and the cathode sheath completely dissipates, restoring the electric field to the undistorted state. Therefore, a typical feature of the 1^1 periodic state is the emergence of a quasisinusoidal SAO between the two adjacent LAOs, as can be seen in Fig. 2(c). Frequency-locking due to competition between different transport processes allows the periodic state to be stabilized over a fairly wide range of control parameters. Further bifurcations occur as R_b is continuously decreased and the number of SAOs increases by one in a period-adding cascade in each oscillation period while the number of LAOs remains constant, because the effect of the ionization processes caused by the residual charge particles becomes more significant and more SAOs are required to release the residual charge particles that were not dissipated in the LAOs. The system will go through 1^2 and 1^3 states successively, which can be seen as Figs. 2(e) and 2(g).

Meanwhile, the APC phenomenon was observed between two adjacent frequency-locking regions, which means that a chaotic band $C^{(n,n+1)}$ will appear between the periodic windows 1^n and 1^{n+1} . This phenomenon has been widely observed and studied in many other physical systems [44–46]. Nonetheless, the APC in discharge plasma systems has been scarcely reported in the literature. The APC phenomenon can be clearly seen in the amplitude bifurcation diagram in Fig. 3. As can be seen, the width of the periodic window decreases with the decrease in R_b . Figure 2(d) shows that the discharge time series of $C^{(1,2)}$ at $R_b = 16.8 \text{ M}\Omega$. As can be observed, the oscillations are nonperiodic although the MMOs structure is maintained. Moreover, the time evolution of the discharge voltage for different R_b within $C^{(1,2)}$ is presented in Fig. 4. When R_b is slightly below the critical value of the periodic window 1^1 , it can be seen from Fig. 4(a) that it resembles the 1^1 periodic state at a first glance. However, the laminar state will be disrupted and rare irregular bursts with the 1^2 MMOs

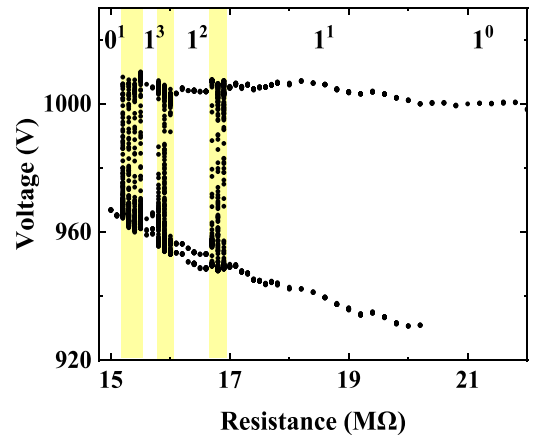


FIG. 3. The amplitude bifurcation diagram. The yellow regions correspond to the intermittently chaotic regions between the transitions of two periodic oscillatory states.

structure will appear, as shown in the gray regions in Fig. 4(a), which is a typical feature of Pomeau-Manneville intermittent chaos [47]. The appearance of 1^2 MMOs structure bursts is due to the fact that the residual charge particles are not fully released after one SAO when R_b is decreased beyond the 1^1 frequency-locking region. With a further decrease in R_b , the random bursts will become more and more frequent until the transition to full chaos [see Fig. 4(b)]. If R_b is continued to decrease after the transition to full chaos, the proportion of the 1^2 MMOs structure bursts in the waveform will continue to increase, as shown in Fig. 4(c), and the system will be eventually transferred to the 1^2 state after passing the critical value. The emergence of the irregular bursts suggests that the chaotic region is “bounded” by the saddle-node bifurcation on both sides. The subsequent intermittently chaotic MMOs bands $C^{(2,3)}$ and $C^{(3,4)}$ were also found between the corresponding periodic windows, as shown in Figs. 2(f) and 2(h). Valuable pieces of information can be also obtained from the time series of the chaotic states. Particularly, there is a feature for an arbitrary chaotic state $C^{(n,n+1)}$ that the time series contains

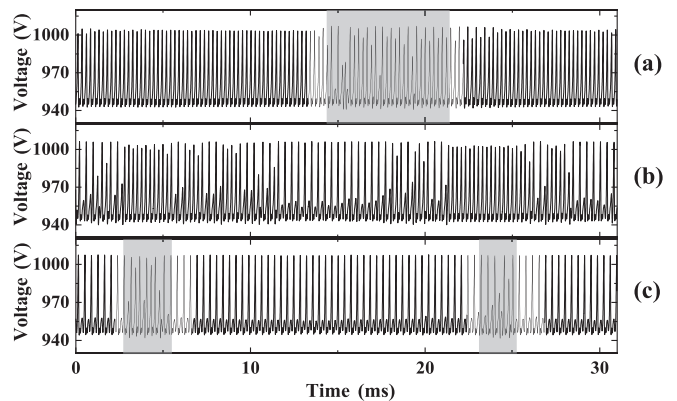


FIG. 4. The intermittently chaotic MMOs in $C^{(1,2)}$ at $R_b =$ (a) $16.9 \text{ M}\Omega$ (b) $16.8 \text{ M}\Omega$, and (c) $16.7 \text{ M}\Omega$ corresponding to the approximate 1^1 state but with rare bursts, fully chaos and approximate 1^2 state but with rare bursts, respectively. The gray regions correspond to the irregular bursts.

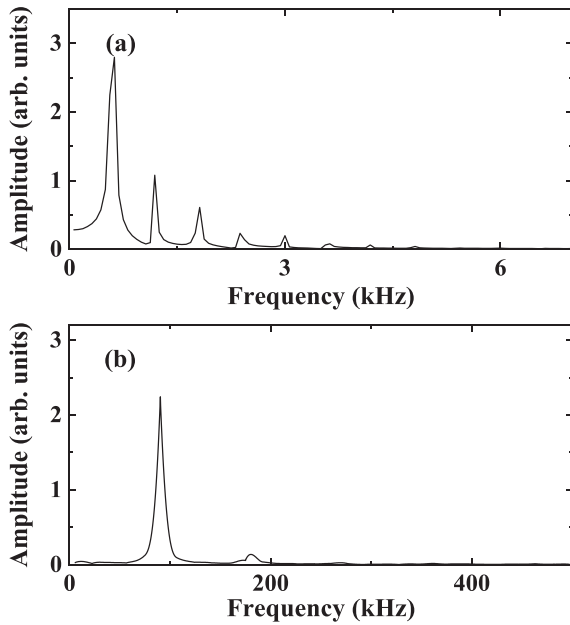


FIG. 5. The FFT spectrum at ballast resistance $R_b =$ (a) 25 M Ω , (b) 15.1 M Ω .

the random mixture of several periodic states $1^1, 1^2, \dots, 1^{n+1}$. This result is similar to the effect that takes place in the electrochemical reaction described in the three-variable mathematical model [24,48] and in the experimental observation of the peroxidase-oxidase reaction [49], which demonstrates the correlation of the different multiple timescales physical systems and the universality of chaos.

Due to the influence of the unavoidable noise and the decrease in the width of the periodic window, the higher-order 1^n periodic states ($n > 3$) were not observed. However, with the further decrease in R_b , there is an increasing number of SAOs separating two successive LAOs and higher-order 1^n MMOs structures can be observed in the evolution of the discharge voltage. As can be seen from Fig. 2(i), the number of the LAOs decreased while the corresponding number of SAOs increased in one MMO unit and there exist up to 1^7 MMOs structures at $R^b = 15.2$ M Ω , which may indicate the theoretical possibility of the existence of the higher-order periodic windows. The state is called $C^{(n,n+1)}$, which means the higher-order chaotic state with uncertain specific order. Eventually, LAOs vanished completely and only SAOs existed in the oscillation waveform, which suggests the system transition to the 0^1 state, as shown in Fig. 2(j). This is due to the fact that in this case the electron production process is so strong that the residual electron cannot be fully dissipated, and the dynamic behavior of the system is determined by the competition between the electron production and loss processes, rather than by the periodic formation and dissipation of the cathode sheath due to the negative differential conductivity. Figure 5 presents the fast Fourier transformation (FFT) spectrum at $R_b =$ (a) 25 M Ω and (b) 15.2 M Ω , which corresponds to the 1^0 and 0^1 states, respectively. As can be ascertained from Fig. 5, the harmonic component of the 0^1 state was significantly reduced, which indicates the oscillation mode transition from the relaxation oscillation to the near-sinusoidal oscillation.

The 0^1 state occupies an extremely narrow parameter range, as shown in Fig. 3, and eventually, the oscillations disappeared and the system transition to a stable glow discharge state took place at about $R_b = 15$ M Ω .

B. Characterization of chaos by the time-series analysis techniques

In this section, the main focus was led on the characteristics of the chaotic behavior between the periodic windows to deeply understand the characteristics and nature of MMOs. Due to the extremely complex nature of the discharge process, it is almost impossible to fully capture the dynamic equations of the system. However, with the development of nonlinear time series analysis techniques, it can be used to reconstruct the phase space of the discrete time series to study the complexity of the chaotic behavior.

First, the information of the discrete time series was extracted by recovering the attractor of the high-dimensional phase space using the phase-space reconstruction method, which is considered to be topologically equivalent to the attractor of the original system according to Takens *et al.* [50]. This method allows the experimentally obtained one-dimensional discrete voltage time series $x(t)$ to be rewritten as a m -dimensional vector $X(t) = (x(t), x(t + \tau), \dots, x(t + (m - 1)\tau))$ by selecting a specified embedding dimension m and time delay τ . By using the phase-space reconstruction technique, it is possible to reproduce the regular, and tangible trajectories in high-dimensional space from complex and irregular discrete time series. It is crucial to choose the appropriate time delay τ and embedding dimension m to restore the topological properties of the original system. In this work, the time delay and embedding dimension were estimated by using average mutual information (AMI) and false nearest neighbor (FNN) algorithm [51], respectively. Figure 6 displays the projection of the reconstructed chaotic attractor at $R_b = 16.8$ M Ω in the reconstructed phase space, where the embedding dimension $m = 5$ and the time delay $\tau = 9\Delta t$.

According to the time series and the corresponding reconstructed phase-space attractor, the dynamics of the system can be described as follows: the trajectory slowly moves around the saddle focus along the unstable manifold with a spiral motion. After several cycles of rotation, the trajectory leaves the vicinity of the saddle focus, which corresponds to the appearance of large amplitude relaxation oscillations, and then is rapidly reinjected into the neighborhood of the saddle focus along with the stable manifold. This process indicates the existence of homoclinic orbits of type Γ^- in the phase space of the system [26]. Due to the slight change in the reinjection trajectory for each cycle, this process will result in a difference in the number of SAOs that is required to escape the saddle focus, which could interpret the coexistence of the different order MMOs structures.

It is well known that a typical characteristic of a determined chaotic system is its sensitivity to the initial state. In other word, the two phase-space trajectories starting from adjacent initial positions will quickly separate, which reflects the unpredictability of the chaotic motion. As an example, the time evolution trajectories of the two neighboring points in

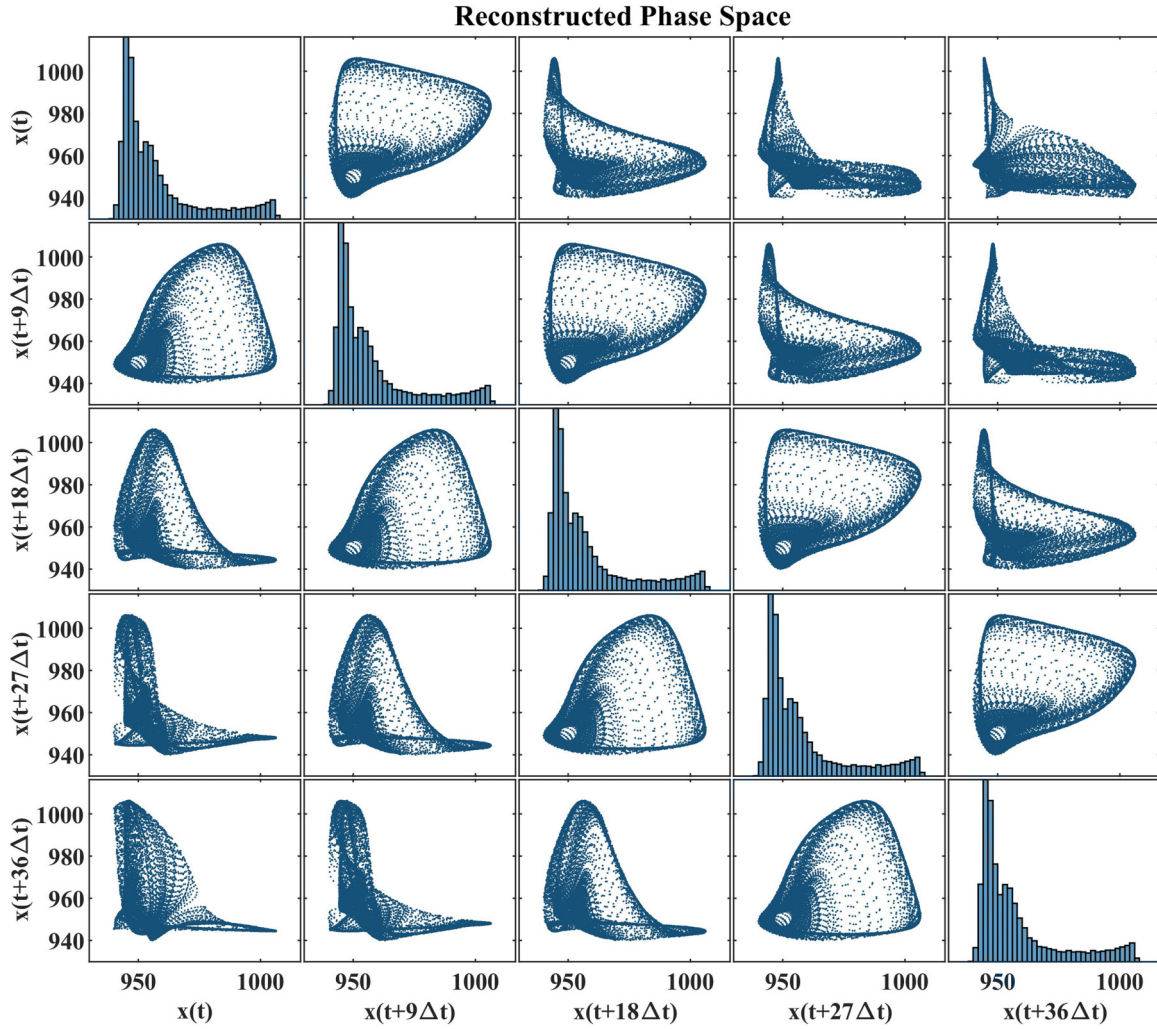


FIG. 6. The reconstructed attractor in the different phase planes for $R_b = 16.8 \text{ M}\Omega$. The embedding dimension $m = 5$ and the time delay $\tau = 9\Delta t$; Δt is the sampling interval of the original series.

the reconstructed phase space at $R_b = 16.8 \text{ M}\Omega$ was tracked, as can be observed in Fig. 7. Here, the initial position was marked by the black solid point and the black (solid) and red (dashed) lines represent the time evolution of the trajectories. The evolution time was $T = 2.5 \text{ ms}$. As can be seen intuitively from Fig. 7, the two trajectories almost overlap at the beginning. As time passes, the trajectories were rapidly separated and then exhibited completely different trends. The above-mentioned result indicates that the system exhibits sensitivity to a slight difference in the initial state. Then, a quantitative analysis of the system’s chaoticity is presented. The rate of separation of infinitesimally close trajectories was characterized by using the Lyapunov exponent λ . For a m -dimensional dynamic system, there will be m Lyapunov exponents $\lambda_1, \lambda_2, \dots, \lambda_m$. It is almost impossible to determine all of the Lyapunov exponents because the governing equations of the real dynamic system are generally not available. In practical applications, one is more concerned with the largest Lyapunov exponent (LLE) λ_1 , which determines how fast the trajectories diverge or converge. Rosenstein *et al.* proposed a practical method to estimate the LLE by calculating

the average divergence rate of the nearest-neighbor point for each point in the reconstructed phase space from the discrete time series as follows [52]:

$$\lambda_1(i) = \frac{1}{i\Delta t} \frac{1}{M-i} \sum_{j=1}^{M-i} \ln \frac{d_j(i)}{d_j(0)}. \quad (1)$$

where i is the time step, Δt denotes the sampling interval, and $d_j(i)$ refer to the distance between the j th pair of nearest-neighbor points after i time steps. Figure 8 presents the average log divergence versus time at $R_b = 16.8, 15.9, 15.5,$ and $15.2 \text{ M}\Omega$, which correspond to the chaotic states $C^{(1,2)}, C^{(2,3)}, C^{(3,4)}$, and $C^{(n,n+1)}$, respectively. It can be seen that the curve initially exhibits an approximately linear relationship, corresponding to the exponential divergence characteristic of the initial adjacent phase-space trajectories. This result confirms the existence of deterministic chaos. With further increase in time, the curve tends to be saturated, which is due to the fact that the average divergence of the trajectories has approached the characteristic scale of the attractor. The red dashed lines indicate the results of the linear fitting for

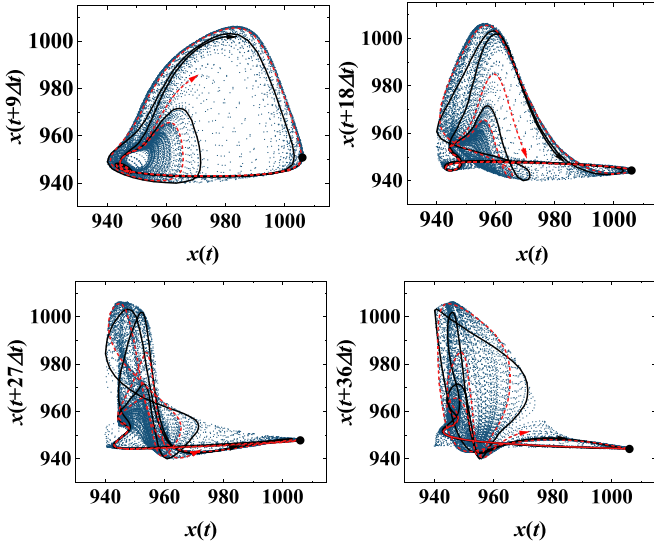


FIG. 7. The time evolution of the trajectories of the two phase-space points that were initially very close to each other in the different phase planes of the reconstructed phase space for $R_b = 16.8 \text{ M}\Omega$. The arrows indicate the direction of the flow.

the exponential divergence region and from the slope, where the values of the corresponding LLE λ_1 were 4.86, 2.31, 1.69, and 1.52, respectively. The existence of positive LLE demonstrates signify the chaotic nature of the irregular time series between the periodic windows. As a specific form of the Poincaré map, the return map (also known as the next maximal amplitude map) $A_n \times A_{n+1}$ was constructed, where A_n corresponds to the n th local maximum of the time series. Figures 9(a)–9(d) illustrate the return map for $R_b = 16.8, 15.9, 15.5,$ and $15.2 \text{ M}\Omega$, respectively, which corresponds to the chaotic states $C^{(1,2)}, C^{(2,3)}, C^{(3,4)},$ and $C^{(n,n+1)}$, respectively. As can be seen from Fig. 9(a), the discrete data points are concentrated on a curve with almost no “thickness.” The

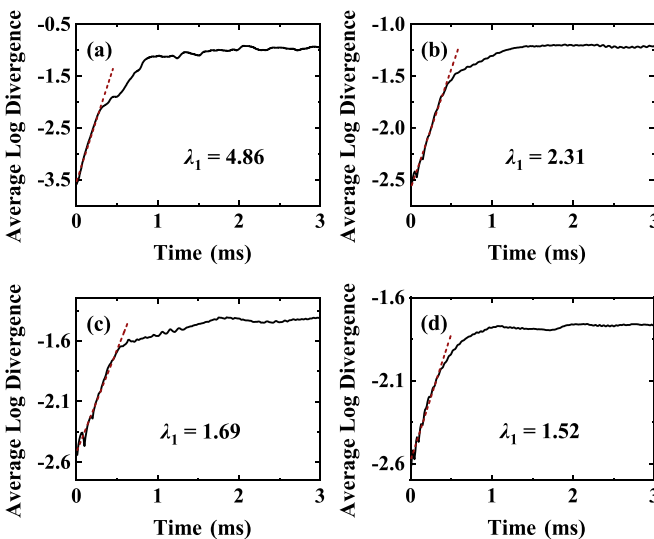


FIG. 8. Average logarithmic divergence for $R_b =$ (a) $16.8 \text{ M}\Omega$, (b) $15.9 \text{ M}\Omega$, (c) $15.5 \text{ M}\Omega$, (d) $15.2 \text{ M}\Omega$, where the slope presents the value of LLE.

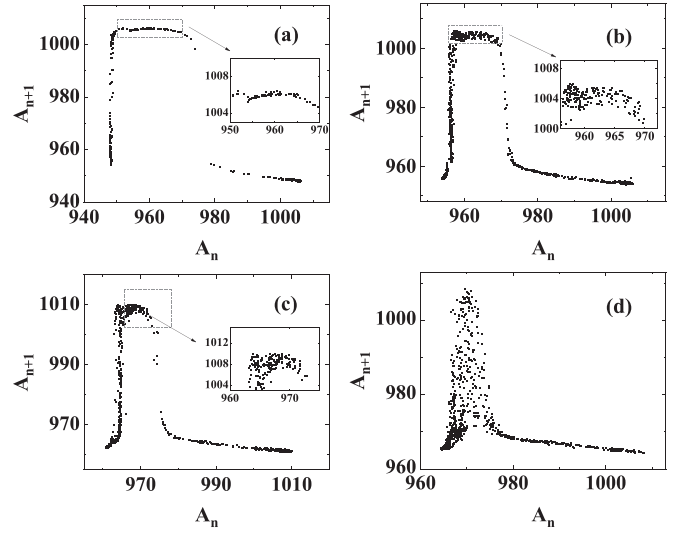


FIG. 9. The return map for $R_b =$ (a) $16.8 \text{ M}\Omega$, (b) $15.9 \text{ M}\Omega$, (c) $15.5 \text{ M}\Omega$, and (d) $15.2 \text{ M}\Omega$.

return maps of $C^{(1,2)}$ state exhibit a one-dimensional unimodal nature with a long tail to the right of the maximum, which is a typical characteristic of MMOs systems [23,53,54]. These results are in line with that the dynamics behavior observed between the periodic windows in low-dimensional chaotic oscillations. Meanwhile, for higher-order chaotic states, a phenomenon that can be significantly observed in Figs. 9(b)–9(d) is that the ratio of the height to the width of the hump becomes larger while the steepness decreases. It is clear that, with the decrease in the steepness of the hump, the probability that an iterate to land on this region of the map function is higher and more iterations are required to leave the channel formed by the hump and the diagonal. Therefore, higher-order MMOs structure will be observed in the higher-order chaotic states. In addition, as can be also noticed in Figs. 9(b) and 9(c) compared with Fig. 9(a), the data points are no longer concentrated on a certain curve and the multiple fold structure appears. For the higher-order chaos state, the multiple folds structure will be more apparent, as shown in Fig. 9(d). The presence of the multiple folds structure as a result of the finite dissipation implies an increase in the complexity of the system. It is well known that the correlation dimension D_{corr} of the chaotic attractors is one of the most important indexes to quantitative characterize the complexity of chaotic systems. To this end, in this work, the Grassberger-Procaccia method based on the reconstructed phase space [55] was used to calculate the correlation dimension. For the m -dimensional reconstructed phase-space system $X(t)$, the correlation integral $C(r)$ is defined as follows:

$$C(r) = \frac{1}{N^2} \sum_{i,j=1}^N \Theta(r - |X_i - X_j|), \quad (2)$$

where N is the number of the vector in the reconstructed phase space and Θ refers to the Heaviside function. $C(r)$ indicates the proportion of the number of the correlated vector pair, which is defined as the vector pair satisfied $r - |X_i - X_j| > 0$, to all possible pairs in the reconstructed phase space. The

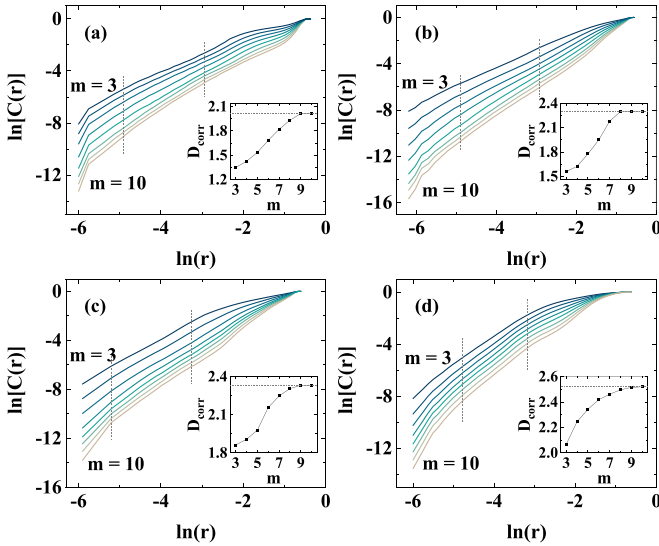


FIG. 10. The effect of the embedding dimension m on the correlation integral $C(r)$ for $R_b =$ (a) 16.8 M Ω , (b) 15.9 M Ω , (c) 15.5 M Ω , and (d) 15.2 M Ω . The inset shows the correlation dimension D_{corr} versus the embedding dimension m .

relation of $C(r)$ and D_{corr} satisfied the following expression,

$$D_{\text{corr}} = \frac{\ln [C(r)]}{\ln r}. \quad (3)$$

Figures 10(a)–10(d) presents the results of $\ln [C(r)]$ vs $\ln r$ for the embedding dimension m in the range of 3–10 for $R_b =$ 16.8, 15.9, 15.5, and 15.2 M Ω , respectively. Considering the influence of the noise and the scale of the strange attractor, the linear scaling is only valid in the intermediate region marked by the dashed lines. Additionally, the relationship between the slope in the linear scaling region and the embedding dimension m is shown in the inset. For a random system, an increase in m leads to a corresponding increase in the slope. On the other hand, for a deterministic chaotic system, as the embedding dimension m increases, the slope converges to a certain noninteger value, i.e., the correlation dimension D_{corr} , indicating the existence of the fractal structure of the chaotic attractor. It can be seen from the inset that, as the embedding dimension increased, D_{corr} gradually increased and eventually became stable. The calculated D_{corr} at different ballast resistances R_b are presented in Table I. It can be seen that the correlation dimension increased for the higher-order chaotic state, indicating that the dissipation of the strange attractor of the system weakened and the complexity increased with the decrease in R_b .

TABLE I. The correlation dimension D_{corr} at different ballast resistance R_b .

R_b	16.8 M Ω	15.9 M Ω	15.5 M Ω	15.2 M Ω
D_{corr}	2.016 ± 0.025	2.303 ± 0.019	2.333 ± 0.022	2.519 ± 0.010

IV. CONCLUSIONS

In the present work, an experimental result was presented showing complex dynamics in the subnormal glow discharge regime of a DC glow discharge system. The experiment was carried out using ballast resistance R_b as the control parameter. The dynamic behavior was characterized by recording the discharge voltage and the period-adding bifurcations sequence of the mixed-mode oscillations state ($1^0 \rightarrow 1^1 \rightarrow 1^2 \rightarrow \dots \rightarrow 1^n \rightarrow 0^1$) was obtained. Meanwhile, an alternating periodic-chaotic phenomenon was observed, i.e., the chaotic oscillations appeared in the transitions between the adjacent periodic states. More specifically, near the critical value of the periodic window, regular periodic oscillations were broken by irregular bursts due to the inverse saddle-node bifurcation and the bursts took place more frequently as the control parameters moved away from the bifurcation point, which is a typical characteristic of Pomeau-Manneville intermittent chaos.

The formation mechanism of the MMOs was discussed and the results suggested that the appearance of LAOs was caused by the periodic formation and dissipation of the cathode sheath due to the existence of the negative differential conductivity, while the appearance of SAOs was due to the frequency locking caused by the competition between the electron production due to the inelastic collisional ionization processes and the electron loss due to the directional movement process towards the anode. With the gradual decrease of R_b , the competition between the two transport processes became more pronounced, leading to an arithmetic increase in the number of small amplitude oscillations. The intermittent chaos beyond the frequency-locking region was due to the residual charge particles not being fully released.

To delve deeply into the complex dynamics of the system, the reconstructed strange attractor which is topologically equivalent to the original system, was recovered by the phase-space reconstruction technique. The emergence of the homoclinic orbits of type Γ^- in the phase space of the system. In this case, small amplitude near-sinusoidal oscillations were detected, which correspond to the slow rotations along with the unstable manifold around the saddle focus. During the fast motion of the trajectory that is reinjected nearby the saddle focus along with the stable manifold, the system exhibited large amplitude relaxation oscillation. Due to the differences in the location of trajectory reinjection along with the slow manifold, the time series of chaotic state $C^{(n,n+1)}$ consisted of a random mixture of different MMO structures $1^1, 1^2, \dots, 1^{n+1}$. Furthermore, the calculation of the largest Lyapunov exponent and correlation dimension was carried out for the chaotic oscillations between the different periodic windows to quantitatively characterize the chaos. The positive largest Lyapunov exponent clearly indicated the existence of the deterministic chaos. Moreover, the presence of the multiple folds in the return map, as well as the results of the calculation of the correlation dimension, implied the increase in the complexity for higher-order chaotic states of the system.

ACKNOWLEDGMENTS

The research has been financially supported by National Natural Science Foundation of China (Grants No. 12205067

and No. 12175050), Project funded by China Postdoctoral Science Foundation (Grant No. 2022M720967) and the Fundamental Research Funds for the Central Universities (Grant No. HIT.OCEF.2022036).

-
- [1] P. Y. Cheung and A. Y. Wong, Chaotic behavior and period doubling in plasmas, *Phys. Rev. Lett.* **59**, 551 (1987).
- [2] Z. Donko and L. Szalai, Chaotic current oscillations with broadband $1/f^\alpha$ spectrum in a glow discharge plasma, *Chaos, Solitons Fractals* **7**, 777 (1996).
- [3] M. Nurujjaman, R. Narayanan, and A. Sekar Iyengar, Parametric investigation of nonlinear fluctuations in a dc glow discharge plasma, *Chaos* **17**, 043121 (2007).
- [4] J. L. Walsh, F. Iza, N. B. Janson, and M. G. Kong, Chaos in atmospheric-pressure plasma jets, *Plasma Sources Sci. Technol.* **21**, 034008 (2012).
- [5] C. Yuan, C. Yesil, J. Yao, Z. Zhou, and I. Rafatov, Transition from periodic to chaotic oscillations in a planar gas discharge-semiconductor system, *Plasma Sources Sci. Technol.* **29**, 065009 (2020).
- [6] P. Alex, M. Perumal, and S. K. Sinha, Coexistence of chaotic and complexity dynamics of fluctuations with long-range temporal correlations under typical condition for formation of multiple anodic double layers in dc glow discharge plasma, *Nonlinear Dyn.* **101**, 655 (2020).
- [7] D. D. Šijačić, U. Ebert, and I. Rafatov, Period doubling cascade in glow discharges: Local versus global differential conductivity, *Phys. Rev. E* **70**, 056220 (2004).
- [8] R. R. Arslanbekov and V. I. Kolobov, Two-dimensional simulations of the transition from Townsend to glow discharge and subnormal oscillations, *J. Phys. D: Appl. Phys.* **36**, 2986 (2003).
- [9] R. Kumar, R. Narayanan, R. Tarey, and A. Ganguli, Characterization of dc glow discharge plasma in co-axial electrode geometry system by nonlinear dynamical analysis tools, *Phys. Plasmas* **30**, 013508 (2023).
- [10] D. Mansuroglu, I. Uzun-Kaymak, and I. Rafatov, An evidence of period doubling bifurcation in a dc driven semiconductor-gas discharge plasma, *Phys. Plasmas* **24**, 053503 (2017).
- [11] D. Dai, X. Zhao, and Q. Wang, Inverse period-doubling bifurcation in an atmospheric helium dielectric barrier discharge, *Europhys. Lett.* **107**, 15002 (2014).
- [12] Z. Chu, J. Yao, C. Yuan, Z. Zhou, A. Kudryavtsev, X. Wang, and Y. Wang, Numerical simulation of the bifurcation-remerging process and intermittency in an undriven direct current glow discharge, *Phys. Rev. E* **106**, 065207 (2022).
- [13] Z. Chu, J. Yao, C. Yuan, Z. Zhou, A. Kudryavtsev, Y. Wang, and X. Wang, Numerical simulation of the hysteresis of the transition from the stationary to oscillatory regime in the low-pressure dc glow discharge, *Phys. Plasmas* **30**, 042304 (2023).
- [14] Ding Weixing, Huang Wei, Wang Xiaodong, and C. X. Yu, Quasiperiodic transition to chaos in a plasma, *Phys. Rev. Lett.* **70**, 170 (1993).
- [15] C. Letellier, A. Dinklage, H. El-Naggar, C. Wilke, and G. Bonhomme, Experimental evidence for a torus breakdown in a glow discharge plasma, *Phys. Rev. E* **63**, 042702 (2001).
- [16] J. Zhang, Y. Wang, and D. Wang, Numerical simulation of torus breakdown to chaos in an atmospheric-pressure dielectric barrier discharge, *Phys. Plasmas* **20**, 082315 (2013).
- [17] P. Y. Cheung, S. Donovan, and A. Y. Wong, Observations of intermittent chaos in plasmas, *Phys. Rev. Lett.* **61**, 1360 (1988).
- [18] D. L. Feng, J. Zheng, W. Huang, C. X. Yu, and W. X. Ding, Type-I-like intermittent chaos in multicomponent plasmas with negative ions, *Phys. Rev. E* **54**, 2839 (1996).
- [19] S. Ghosh, P. Kumar Shaw, A. Sekar Iyengar, M. Janaki, D. Saha, A. Michael Wharton, and V. Mitra, Experimental evidence of intermittent chaos in a glow discharge plasma without external forcing and its numerical modelling, *Phys. Plasmas* **21**, 032303 (2014).
- [20] D. Bakeš, L. Schreiberová, I. Schreiber, and M. J. Hauser, Mixed-mode oscillations in a homogeneous pH-oscillatory chemical reaction system, *Chaos* **18**, 015102 (2008).
- [21] S. Chakraborty and S. K. Dana, Shil'nikov chaos and mixed-mode oscillation in Chua circuit, *Chaos* **20**, 023107 (2010).
- [22] K. Shimizu, Y. Saito, M. Sekikawa, and N. Inaba, Complex mixed-mode oscillations in a bonhoeffer-van der Pol oscillator under weak periodic perturbation, *Phys. D (Amsterdam, Neth.)* **241**, 1518 (2012).
- [23] L. F. Olsen and A. Lunding, Chaos in the peroxidase-oxidase oscillator, *Chaos* **31**, 013119 (2021).
- [24] M. T. Koper and P. Gaspard, The modeling of mixed-mode and chaotic oscillations in electrochemical systems, *J. Chem. Phys.* **96**, 7797 (1992).
- [25] J. Guckenheimer and I. Lizarraga, Shilnikov homoclinic bifurcation of mixed-mode oscillations, *J. Appl. Dyn. Syst.* **14**, 764 (2015).
- [26] A. Arneodo, F. Argoul, J. Elezgaray, and P. Richetti, Homoclinic chaos in chemical systems, *Phys. D (Amsterdam, Neth.)* **62**, 134 (1993).
- [27] K. Shimizu, M. Sekikawa, and N. Inaba, Experimental study of complex mixed-mode oscillations generated in a Bonhoeffer-van der Pol oscillator under weak periodic perturbation, *Chaos* **25**, 023105 (2015).
- [28] M. Sekikawa, T. Kousaka, T. Tsubone, N. Inaba, and H. Okazaki, Bifurcation analysis of mixed-mode oscillations and Farey trees in an extended Bonhoeffer-van der Pol oscillator, *Phys. D (Amsterdam, Neth.)* **433**, 133178 (2022).
- [29] N. Inaba, T. Kousaka, T. Tsubone, H. Okazaki, and H. Ito, Mixed-mode oscillations from a constrained extended Bonhoeffer-van der Pol oscillator with a diode, *Chaos* **31**, 073133 (2021).
- [30] W. Nicola, P. J. Hellyer, S. A. Campbell, and C. Clopath, Chaos in homeostatically regulated neural systems, *Chaos* **28**, 083104 (2018).
- [31] F. Zhan, S. Liu, X. Zhang, J. Wang, and B. Lu, Mixed-mode oscillations and bifurcation analysis in a pituitary model, *Nonlinear Dyn.* **94**, 807 (2018).
- [32] E. J. Doedel, L. Pando, and L. Carlos, Multiparameter bifurcations and mixed-mode oscillations in Q-switched CO₂ lasers, *Phys. Rev. E* **89**, 052904 (2014).

- [33] E. J. Doedel and C. L. Pando L., Rare events in mixed-mode oscillations from weakly coupled lasers, *Phys. Rev. E* **100**, 052204 (2019).
- [34] A. Dolcemascolo, A. Miazek, R. Veltz, F. Marino, and S. Barland, Effective low-dimensional dynamics of a mean-field coupled network of slow-fast spiking lasers, *Phys. Rev. E* **101**, 052208 (2020).
- [35] C. Zhang and Q. Tang, Complex periodic mixed-mode oscillation patterns in a Filippov system, *Mathematics* **10**, 673 (2022).
- [36] I. Bashkirtseva and L. Ryashko, Mixed-mode self-oscillations, stochastic excitability, and coherence resonance in flows of highly concentrated suspensions, *Nonlinear Dyn.* **102**, 1837 (2020).
- [37] T. Braun, J. A. Lisboa, and J. A. C. Gallas, Evidence of homoclinic chaos in the plasma of a glow discharge, *Phys. Rev. Lett.* **68**, 2770 (1992).
- [38] T. Braun and J. A. Lisboa, Characterization of homoclinic chaos in a glow discharge through return maps, *Int. J. Bifurcation Chaos Appl. Sci. Eng.* **04**, 1483 (1994).
- [39] T. Hayashi, Mixed-mode oscillations and chaos in a glow discharge, *Phys. Rev. Lett.* **84**, 3334 (2000).
- [40] E. Pugliese, R. Meucci, S. Euzzor, J. G. Freire, and J. A. Gallas, Complex dynamics of a dc glow discharge tube: Experimental modeling and stability diagrams, *Sci. Rep.* **5**, 8447 (2015).
- [41] Y. Zhang, Y. Qin, G. Zhao, and J. Ouyang, Time-resolved analysis and optical diagnostics of Trichel corona in atmospheric air, *J. Phys. D: Appl. Phys.* **49**, 245206 (2016).
- [42] R. Cui, F. He, J. Miao, and J. Ouyang, Experimental study on self-pulsing in flow-induced atmospheric pressure plasma jet, *Phys. Plasmas* **24**, 103524 (2017).
- [43] I. Stefanović, T. Kuschel, N. Škoro, D. Marić, Z. L. Petrović, and J. Winter, Oscillation modes of direct current microdischarges with parallel-plate geometry, *J. Appl. Phys.* **110**, 083310 (2011).
- [44] P. C. Rech, Period-adding structures in the parameter-space of a driven Josephson junction, *Int. J. Bifurcation Chaos Appl. Sci. Eng.* **25**, 1530035 (2015).
- [45] V. S. Piassi, A. Tufaile, and J. C. Sartorelli, Period-adding bifurcations and chaos in a bubble column, *Chaos* **14**, 477 (2004).
- [46] T.-F. Li, Z.-G. Su, K. Luo, and H.-L. Yi, Transition to chaos in electro-thermo-convection of a dielectric liquid in a square cavity, *Phys. Fluids* **32**, 013106 (2020).
- [47] Y. Pomeau and P. Manneville, Intermittent transition to turbulence in dissipative dynamical systems, *Commun. Math. Phys.* **74**, 189 (1980).
- [48] A. L. Kawczyński and P. E. Strizhak, Period adding and broken Farey tree sequence of bifurcations for mixed-mode oscillations and chaos in the simplest three-variable nonlinear system, *J. Chem. Phys.* **112**, 6122 (2000).
- [49] M. J. Hauser and L. F. Olsen, Mixed-mode oscillations and homoclinic chaos in an enzyme reaction, *J. Chem. Soc., Faraday Trans.* **92**, 2857 (1996).
- [50] F. Takens, Detecting strange attractors in turbulence, in *Dynamical Systems and Turbulence, Warwick 1980: Proceedings of a Symposium Held at the University of Warwick 1979/80* (Springer, 2006), pp. 366–381.
- [51] C. Rhodes and M. Morari, False-nearest-neighbors algorithm and noise-corrupted time series, *Phys. Rev. E* **55**, 6162 (1997).
- [52] M. T. Rosenstein, J. J. Collins, and C. J. De Luca, A practical method for calculating largest Lyapunov exponents from small data sets, *Phys. D (Amsterdam, Neth.)* **65**, 117 (1993).
- [53] R. Raghavan and G. Ananthakrishna, Long tailed maps as a representation of mixed mode oscillatory systems, *Phys. D (Amsterdam, Neth.)* **211**, 74 (2005).
- [54] N. M. Awal and I. R. Epstein, Period-doubling route to mixed-mode chaos, *Phys. Rev. E* **104**, 024211 (2021).
- [55] P. Grassberger and I. Procaccia, Characterization of strange attractors, *Phys. Rev. Lett.* **50**, 346 (1983).